16

Mathematical Modelling of Structure Formation of Discrete Materials

Lyudmila Ryabicheva and Dmytro Usatyuk
Volodymyr Dahl East Ukrainian National University
Ukraine

1. Introduction

The mathematical modelling of different processes and events may be reduced, in most cases, to formulation of boundary-value problems for defined systems of differential equations. Series of statements and approximate methods for solving of such equations were developed by many authors. The most development have obtained variation methods, direct methods of mathematical physics and integral equation methods. These methods have specific capabilities and peculiarities, expanded class of observed problems, but were not completely eliminated most of principal contradictions. Nowadays, the most challenging method is finite element method (FEM). It has reached so high stage of development and popularity that can be no doubts of existence another approach competitive in capabilities and simplicity of realization (Segal et al., 1981; Wagoner & Chenot, 2001).
The advantages of finite element method are free selection of nodal points, arbitrary shape of region and boundary conditions, simplicity of generalization for different models of bodies and problems of any dimensionality, natural accounting the non-uniformity of properties and other local effects, using of standard programs for a whole class of problems. A finite element method is well grounded, the equivalence of its different forms to differential and variation formulations and, also, to special cases of Ritz method, Bubnov-Galerkin method and least-squares method established (Zienkiewicz & Taylor, 2000).
The first step of numerical solution is discretization of medium that allows reducing the problems with infinite number of degrees of freedom typical to continuous approach, to problems with finite number of unknown variables. Usually, discretization is including selection of certain number of nodal points with following implementation of two types of variables – nodal variables and special functions that are approximating the distributions of target parameters inside elements. In such case, the independent parameters are the nodal variables and distributions of target parameters that are determined by them (Zienkiewicz & Taylor, 2000).
During finite element approximation the integration procedure is replaced by more simple algebraic operators expressed through nodal variables by summation on elements. Partial differential equations are replaced by system of algebraic equations written for sequence of nodes and special functions by functions for finite number of nodal variables. The subsequent calculation of target values and determination of parameters of state may be executed by standard methods of numerical analysis. The general requirements for selection of finite elements and approximating functions are determined by convergence criterions of FEM (Zienkiewicz & Taylor, 2000).

The implementations of FEM to solving of technological tasks of plasticity theory and modelling of physical and mechanical properties associated with metal forming processes are described below. Large deformations specific for such processes are leading to changing the geometry of region and properties of material. In these cases most of peculiarities of plastic state that produce difficulties of numerical solution are appeared (Petrosjan, 1988; Wagoner & Chenot, 2001).

2. Solving of the non-stationary nonlinear coupled thermal-structural problem by finite element method

The behaviour of powder porous bodies at plastic deformation and high temperatures is characterizing by substantial non-uniformity that makes necessary application of numerical methods (Petrosjan, 1988). Nonlinear character of deformation and substantial non-uniformity of deformed state in combination with large temperature gradients are leading to the necessity of solving a non-stationary nonlinear coupled thermal-structural problem. The matter of this problem is that forming process of detail depends not only from degree of deformation and strain rate but, also, from temperatures which continuously changing by nonlinear laws (Wagoner & Chenot, 2001; Hallquist, 2006; Ryabicheva & Usatyuk, 2006). The sequence of solving of non-stationary nonlinear coupled thermal-structural problem consists of the followings steps: problem formulation, discretization scheme, computational procedure and computer visualization of results.

The eight node linear tetrahedron-shaped element has used for analysis of stress-strain state, temperature distributions and physico-mechanical properties. The fundamental idea is that five nodal points of element have common coordinates and each projection of their displacement is described by one equation (Hallquist, 2006). According to (Segal et al., 1981), a minimum of functional is corresponding to actual velocity field:

$$J = \iiint_V \sigma_{ij} e_{ij} dV - \iint_{S_k} p_i v_i dS, \tag{2.1}$$

where σ_{ij}, e_{ij} - are stress tensor and strain rate tensor;

p_i - are pressures applied on external border;

v_i - are velocities of displacements of points under the action of external forces;

V - is volume of body;

S_k - is surface of body.

During a finite-element approximation integration is replaced by summing up on elements and minimization of function (4.1) results in the system of equations:

$$[K]\{\dot{X}\} = \{p\}, \tag{2.2}$$

where $[K] = [K(X, \dot{X})]$ - is global stiffness matrix of system;

$\{p\}$ - are column-matrices of nodal velocities and forces.

Dependences between nodal velocities and strain rates and, also, stresses into element are looking like (Segal et al., 1981):

$$\{e\}^{(e)} = [B]\{v\}^{(e)}, \quad \{\sigma\}^e = [K]\{v\}^e. \tag{2.3}$$

Matrices [B] and [K] are determined by standard technique. The dependence between stresses and strain rates, determined by matrix [D], obtained using the following relation (Skorokhod, 1973; Segal et al., 1981; Shtern et al., 1982):

$$\sigma_{ij} = \beta\left[\phi e_{ij} + \left(\psi - \frac{1}{3}\phi\right)e\delta_{ij}\right], \tag{2.4}$$

where $\beta = \dfrac{\sqrt{1-\theta}\tau_0}{\sqrt{\phi\gamma^2 + \psi e^2}}$;

θ - is porosity of material;

ϕ, ψ - are porosity functions (Shtern et al., 1982): $\phi = (1-\theta)^2$, $\psi = \dfrac{2}{3}\dfrac{(1-\theta)^3}{\theta}$;

τ_0 - is ultimate intensity of deviatoric stresses for basic material of porous body.

The visco-plastic medium investigated during plastic deformation at high temperatures according to recommendations of Kachanov L.M. (Kachanov, 1969). A substantial metal flow is typical for visco-plastic medium at the certain load and flow velocity depends on viscosity of medium. In case of axis-symmetrical problem (Zienkiewicz & Taylor, 2000; Wagoner & Chenot, 2001):

$$[D] = \begin{bmatrix} \frac{4}{3}\phi + \psi & \psi - \frac{2}{3}\phi & \psi - \frac{2}{3}\phi & 0 \\ \psi - \frac{2}{3}\phi & \frac{4}{3}\phi + \psi & \psi - \frac{2}{3}\phi & 0 \\ \psi - \frac{2}{3}\phi & \psi - \frac{2}{3}\phi & \frac{4}{3}\phi + \psi & 0 \\ 0 & 0 & 0 & 2\phi \end{bmatrix}. \tag{2.5}$$

The kinetic equation of porosity changing in visco-plastic area looks like (Shtern et al., 1982):

$$\frac{d\theta}{dt} = (1-\theta)\left(\frac{\phi H\sigma}{\psi T} + \frac{\sigma}{\psi}\right), \tag{2.6}$$

where H - is intensity of shear strain rate;

σ - is current normal stress;

$T = \left(\frac{1}{2}\sigma'_{ij}\sigma'_{ij}\right)^{1/2}$ - is shear stress intensity.

Beginning of plastic flow corresponds to implementation of condition (Shtern et al., 1982):

$$f \equiv \psi T^2 + \phi\sigma^2 - \sigma_s^2 = 0, \tag{2.7}$$

where σ_s - is yield stress at linear tension $\left(\sigma_s = \sqrt{3}\Gamma_s\right)$.

System of equations (2.2) is algebraically nonlinear relatively to $\{\dot{X}\}$ and in relation to $\{X\}$ it is a system of differential equations. The step-by-step loading method has used for its integration. In such case the displacement of deforming element is divided on the row of steps with value Δh . A nonlinear algebraic equations system (2.2) is solving during each of steps for determination of $\{\dot{X}\}$. The values equal to product of time step to average velocity between respective load steps are added to coordinates on previous time step for determination of nodal coordinates.

In case of time step size is quite small, the velocity distribution allows to define coordinates and deformation of nodal points at the end of step (Zienkiewicz & Taylor, 2000):

$$\begin{aligned} x_i(t+\Delta t) &= x_i(t) + V_i(t)\Delta t, \\ \varepsilon_{ij}(t+\Delta t) &= \varepsilon_{ij}(t) + \varepsilon_{ij}(t)\Delta t. \end{aligned} \tag{2.8}$$

Changes of shape and properties of material are calculating in such way and attained accuracy is usually sufficient for practical purposes.

The important feature of plastic deformation dependences is that they are not dependent directly on time. Therefore, a displacement of deforming element may be an internal time of system. An iteration process proceeds to stopping of change $\{\dot{X}\}$ and $\{X\}$ with given accuracy. Changing of temperatures on the section of sample at high temperature deformation has determined using the heat conductivity law for each element.

Thus on each load step the analysis of interaction of contact surfaces for elements inside a sample or in contact with surface of instrument was executed, because contact interaction allows determination of heat conductivity only for inner and contacting elements (Segal et al., 1981; Wagoner & Chenot, 2001; Hallquist, 2006; Ryabicheva & Usatyuk, 2006).

The Fourier differential equation was implemented for heat conductivity analysis (Wagoner & Chenot, 2001; Ryabicheva & Usatyuk, 2006):

$$k_T\left(\frac{\partial^2 T}{\partial x^2}+\frac{\partial^2 T}{\partial y^2}+\frac{\partial^2 T}{\partial z^2}\right)dV = C\rho\frac{\partial T}{\partial \tau}dV\,, \tag{2.9}$$

where k_T – is total coefficient of heat conductivity;

C – is specific heat capacity;

ρ – is density of material;

T – is temperature, K;

τ – is time of load step.

A minimum of heat conductivity functional is corresponding to each loading step (Wagoner & Chenot, 2001; Ryabicheva & Usatyuk, 2006):

$$Q = \iiint_V k_T\left(\frac{\partial^2 T}{\partial x^2}+\frac{\partial^2 T}{\partial y^2}+\frac{\partial^2 T}{\partial z^2}\right)dV\,, \tag{2.10}$$

where k_T – is total coefficient of heat conductivity.

Integration of functional (2.10) is replaced by summing up on elements. A time step should be selected small enough in order to ensure homogeneous distribution of temperature and stationary heat transfer inside all elements. Solving of algebraic equation systems has

performed by Gauss method. A maximal change of parameters in any of elements should not exceed some value stipulated by strength properties of material.
Thus, the minimization procedure of functionals (2.1) and (2.10) for non-stationary, nonlinear and non-isothermal processes of deformation of powder porous body consists of solving of linear algebraic equation systems with verification of convergence criterion. The indicated procedure is repeating on each time step for all sequential stages of calculation.
The LS-DYNA 971 solver has used for solving the above mentioned problems.

3. Mathematical modeling and forecasting of mechanical properties of single- and multi-component powder materials

3.1 Mathematical model

The mathematical model of material that proposed for modelling of physico-mechanical properties of porous body is presented by system of constitutive equations that are describing physical and mechanical properties of components.
The finite elements that describe different components of materials are placed in a common mesh. It allows the possibility of taking into account interactions between components. The input data are volume fractions of components, their property in compact state, and also specified value of porosity. The elasto-plastic model of material is applied to all components. The independent parameters are nodal displacements (Segal et al., 1981).
The strain intensities ε_i and strain rates $\dot{\varepsilon}_i$ inside each element are defined through projections of nodal displacements onto the coordinate axes (Segal et al., 1981):

$$\varepsilon_{ix} = \frac{\sum_{\lambda=1}^{N} \frac{\partial u_x^\lambda}{\partial x}}{N}, \qquad \varepsilon_{iy} = \frac{\sum_{\lambda=1}^{N} \frac{\partial u_y^\lambda}{\partial y}}{N}, \qquad \varepsilon_{iz} = \frac{\sum_{\lambda=1}^{N} \frac{\partial u_z^\lambda}{\partial z}}{N},$$

$$\varepsilon_i = \frac{\sqrt{2}}{3}\sqrt{(\varepsilon_{ix}-\varepsilon_{iy})^2 + (\varepsilon_{iy}-\varepsilon_{iz})^2 + (\varepsilon_{iz}-\varepsilon_{ix})^2}, \quad \dot{\varepsilon}_i = \frac{d\varepsilon_i}{dt}. \tag{2.11}$$

where λ – is the node number;
N – is the number of nodes in a finite element;
$u_x^\lambda, u_y^\lambda, u_z^\lambda$ – are projections of nodal displacements onto the coordinate axes;
$\varepsilon_{ix}, \varepsilon_{iy}, \varepsilon_{iz}$ – relative deformations of finite element onto the coordinate axes.

Taking into account the thermo-mechanical coefficients, the Cowper and Symonds equation for stress intensity σ_i inside a finite element looks like (Hallquist, 2006):

$$\sigma_i = \left[1 + \left(\frac{\dot{\varepsilon}_i}{C}\right)^{\frac{1}{p}}\right](\sigma_0 + \beta E \varepsilon_i). \tag{2.12}$$

where σ_0 – is the initial yield stress of a component;
E – is the Young modulus;
$\beta = k_t k_\upsilon k_\varepsilon$ – is the hardening coefficient of component;
C, p – are arbitrary constants.

From the condition of equality of resultant displacements follows that after meshing of finite elements with different properties to common mesh, values of stress intensity, deformation intensity and strain rate at neighbour elements describing different components of material will be different. It means that values of σ, ε, E, Poisson's ratio v and density ρ in the given area of sample may be expressed in the following way (Ryabicheva & Usatyuk, 2007):

$$\sigma = \frac{\sum_{j=1}^{n} \sigma_j}{n}, \quad \varepsilon = \frac{\sum_{j=1}^{n} \varepsilon_j}{n}, \quad E = \frac{\sigma}{\varepsilon}, \quad v = \frac{\varepsilon_{xy}}{\varepsilon_z}, \quad \rho = \frac{\sum_{j=1}^{n} \rho_j}{n \sum_{i=1}^{m} \delta_i}. \tag{2.13}$$

where n – is the number of finite elements in a given area;

ε_{xy}, ε_z – are the radial and axial deformations;

m – is the number of components in the material;

δ_i – is the volume fraction of component.

It is significant that in the proposed model porosity is described as a component of powder material and zero-elements are used for its modelling. The volume fraction of zero-elements is equal to given porosity of the material.

3.2 Initial data

The distributions of stress intensity, degree of deformation, strain rate, temperature and density at the deforming process, estimation of quality of manufactured items have been performed during mathematical modelling of extrusion of rod-shaped billet with predetermined complex of mechanical properties.

The porous fibrous sample with density 8.75 g/cm^3 obtained by pressing of copper fibres with diameter 0.8-1.3 mm and 6-12 mm length have used as initial billet. The finite element model of extrusion of porous fibrous pressing is presented on Fig. 3.1, a. A cylindrical graphite press-washer 2 for filling out the cavity of working part of matrix 4 at the end of extrusion was placed between punch 1 and initial billet 3 for removing finished product from a matrix without butt-end (Fig. 3.1, b).

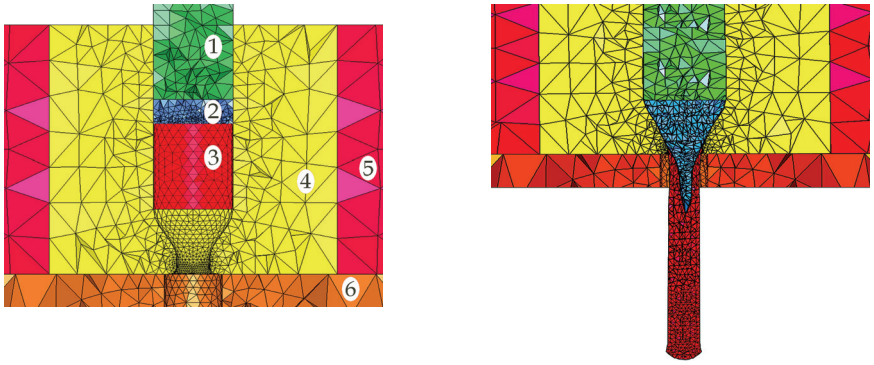

a) b)

Fig. 3.1. The finite element model of extrusion: a - is the initial position; b – is the operation-terminating position: 1 - is the upper puncheon; 2 - is the press-washer; 3 - is the initial pressing; 4 - is the matrix; 5- is the bandage; 6- is the lower plate

The temperature on the beginning of extrusion is 920^{0}C, friction coefficient is 0.15. The diameter of porous fibrous pressing is 23.7 mm, height - 30 mm. The density of graphite press-washer is 2.2 g/cm^3. The diameter of calibrating hole in the matrix was equal to 12.9 mm, 9.1 mm and 6 mm, the reduction ratio was 3.6, 7.3 and 16.8, respectively. A detailed analysis of stress-strain state was performed in three sections passing through the beginning (Fig. 3.2, section 1-1), middle part of deformation zone (Fig. 3.2, section 2-2) and output of matrix 4 (Fig. 3.2, section 3-3).

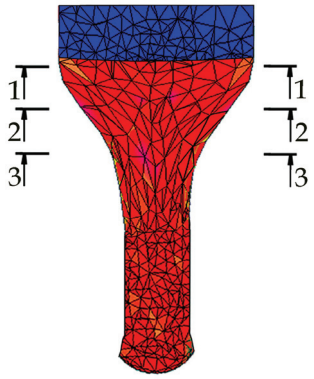

Fig. 3.2. The investigated sections

3.3 Modelling of stress-strain state and distribution of temperatures during extrusion

The stress-strain state picture is almost the same with all reduction ratio investigated, however, at λ = 16.8 the values of stress intensity and hydrostatic pressure are much higher then at λ = 3.6 and 7.3 (Fig. 3.3, a, b). In such conditions the distribution of stress intensity by section of pressing from axis to wall of matrix is more uniform. Its maximal value 145 MPa was reached at the output of deformation zone near the wall of matrix. The existence of gradients of additional stresses, tensile stresses near the walls of matrix and compression stresses in the inner layers of metal leads to complex character of hydrostatic pressure changing by section of billet. The value of hydrostatic pressure has grown up and become 1380 MPa (Fig. 3.3, b).

Obviously, the maximal point at radius of billet r = 2 - 4 mm is corresponding to beginning formation of flow-through flaw in the billet, that is well concordant with one of basic laws of metal forming theory about the flow of metal in the direction of least resistance – by the axis of matrix and, also, corresponding to distribution of strain intensity (Fig. 3.3, d).

The presence of tensile deformations in central part of sample ensures larger value of strain intensity that diminishing to the walls of matrix due to the influence of friction. Increasing of longitudinal tensile normal stresses from axis to wall of matrix causes decreasing of transversal layers thickness near the wall and their thickening at the central area of billet. The strain rate intensity in sections 1-1 and 2-2 has conditioned by proximity of certain volumes to elastic zones of cylindrical segment of container and calibrating segment of matrix. It should be noted that difference between strain rates in sections 2-2 and 3-3 becoming lower with growing of reduction ratio that testifies increasing of stiffness of stress-strain state while increasing of reduction ratio.

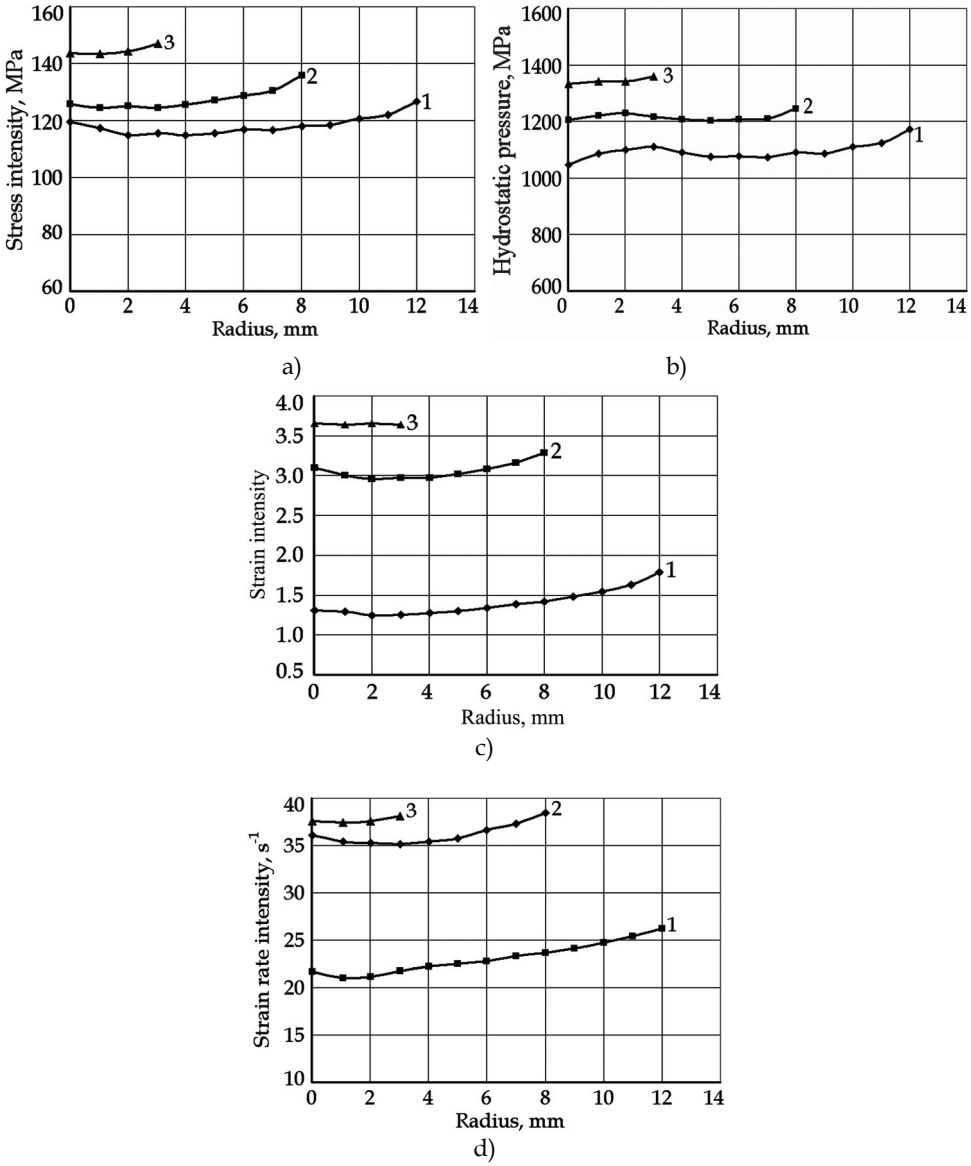

Fig. 3.3. The distribution of stress intensity (a), hydrostatic pressure (b), strain intensity (c), strain rate intensity (d) at λ=16.8: 1– is the section 1–1; 2– is the section 2–2; 3 – is the section 3–3

Computer modelling of stress-strain state during extrusion of fibrous pressing is corresponding to results of analysis of common scheme of changing the coordinate grid by its state in the beginning, middle and the end of deformation zone in experimental investigation (Fig. 3.4).

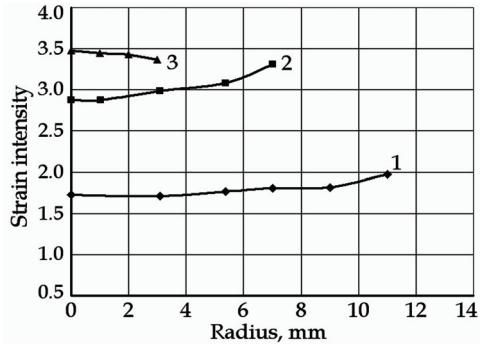

a)

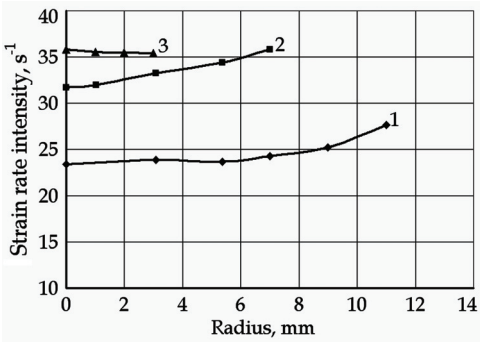

b)

Fig. 3.4. The distribution of strain intensity (a) and strain rate intensity (b) by sections:
1 – is the section 1–1; 2 – is the section 2-2; 3 – is the section 3-3

The maximum values and most uniform distribution of strain intensity and strain rate intensity have reached at section 3-3 that ensures production of sample of given diameter. The distributions of temperatures for all of three reduction ratios into investigated sections are similar (Fig. 3.4).

It should be noted that temperature goes down in section 1-1 only in the 3 mm layer of pressing due to heat transfer to the matrix at all of three reduction ratios. However, the temperature decreases more intensively to 650 °C at $\lambda = 16.8$ (Fig. 3.5). Decreasing of temperature in the centre of deformation zone (section 2-2) goes more intensively due to growth of reduction ratio that is related to increasing of contact area of pressing with walls of matrix. The most rapidly it appears in section 3-3 when at the small diameter of article happens sharp falling of temperature by whole section. The reasons of such temperature changes are heat conductivity processes in layers of pressing at extrusion and between pressing and walls of matrix.

The distribution of density at different reduction ratios is presented on Fig. 3.6. The density is falling down while increasing the distance from centre of sample to circumference of the sample. Specifically, at $\lambda = 3.6$ the density fell to 8.70 g/cm^3, at $\lambda = 7.3$ to 8.87 g/cm^3. The

density is slightly decreasing to 8.93 g/cm^3 at $\lambda = 16.8$ and almost constant by section of sample.

The shear stress intensity, that is growing up while increasing of reduction ratio, have defined for estimating the consolidation of fibres at current density of samples (Fig. 3.7).

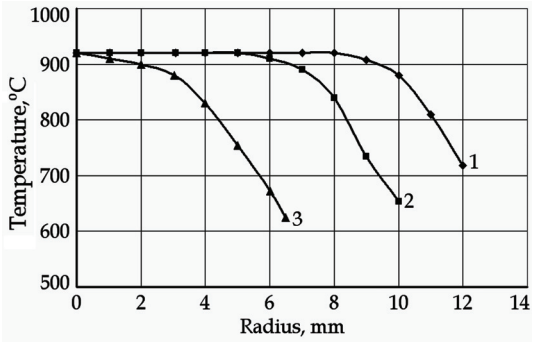

a)

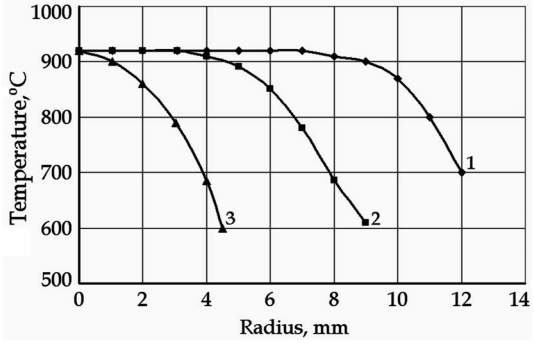

b)

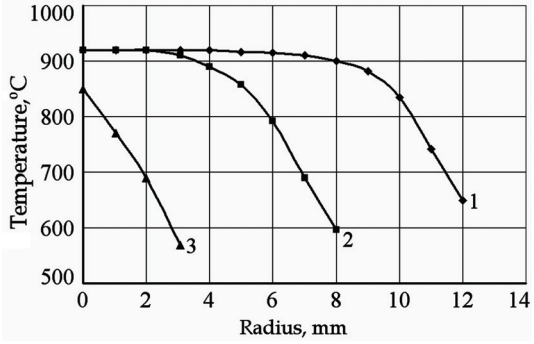

c)

Fig. 3.5. The distributions of temperatures by sections of billet during extrusion: $\lambda = 3.6$ (a), $\lambda = 7.3$ (b), $\lambda = 16.8$ (c): 1 – is the section 1–1; 2 – is the section 2–2; 3 – is the section 3–3

A comparison of shear stress intensity performed with critical shear stress τ_{cr} determined by formula:

$$\tau_{cr} = \frac{\sigma_T}{\sqrt{3}}, \tag{3.1}$$

where σ_T - is the yield stress at given temperature and strain rate conditions.

It should be noted that at $\lambda = 3.6$ the intensity of shear stress is lower than critical shear stress, at $\lambda = 7.3$ the value of τ is a bit lower than τ_{cr} that testifies to incomplete consolidation of fibres, and at $\lambda = 16.8$ its value much higher than τ_{cr}. A high hydrostatic pressure within 1000-1380 MPa at the reduction ratio $\lambda = 16.8$ ensures full consolidation of fibres at extrusion and production of nonporous fully consolidated material that meeting the requirements of standard. These data have been verified by mechanical properties of material obtained experimentally.

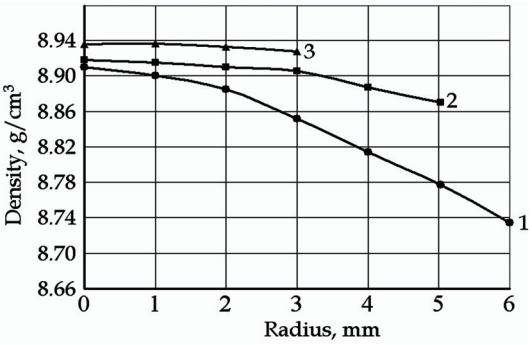

Fig. 3.6. Distributions of density by sections of copper sample: 1 - λ=3.6; 2 - λ=7.3; 3 - λ=16.8

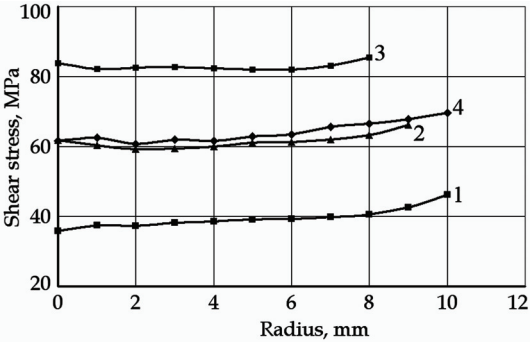

Fig. 3.7. Shear stress intensity: 1 – λ = 3.6; 2 – λ = 7.3; 3 – λ = 16.8; 4 – is a critical shear stress

Thus, modelling of direct extrusion of initial fibrous pressing with the density of 8.75 g/cm^3 has shown that density conformed to density of compact material obtained at the reduction ratio 16.8 ensuring complete consolidation of fibres. However, finite element simulation

allowed identifying defects of material flow similar to experimental results (Fig. 3.8). It has established that flow-through flaw appears on upper end of sample at all reduction ratios.

a) b)

Fig. 3.8. The flow-through flaw on after end (a) and loosening on exposed face (b) of samples obtained from fibrous pressing

Evolution of flow-through flaw at the reduction ratio 16.8 is presented on Fig. 3.9. The flow-through flaw does not appear during the initial stages of deformation (Fig. 3.9, a, b) while metal did not fill in the working segment of matrix. A flow-through flaw nucleates at transferring of metal to deformation zone into the centre of pressing (Fig. 3.9, c). A slight increasing of hydrostatic pressure on its edges observed. A flow-through flaw spreads deep into billet by the end of extrusion (fig. of a 3.9, d, e) and its depth l_{sk} is depending on the reduction ratio.

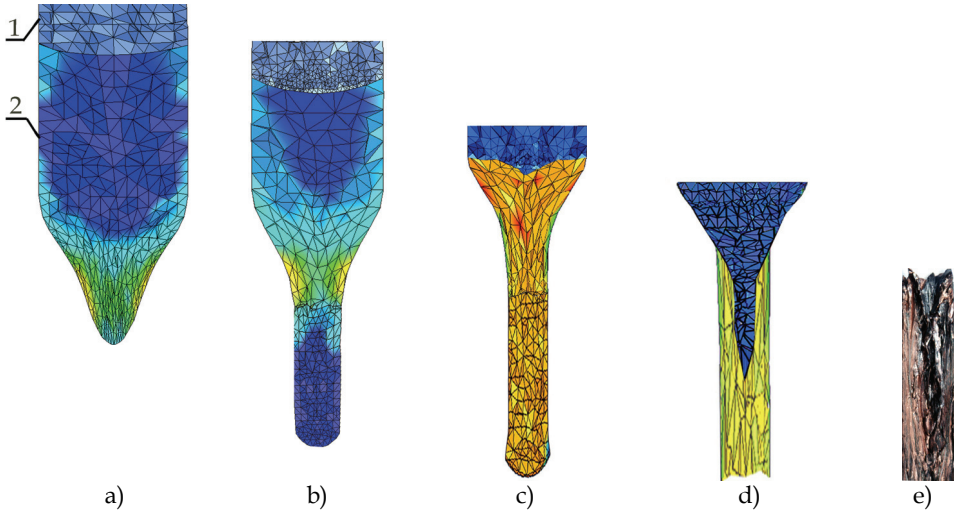

a) b) c) d) e)

Fig. 3.9. The evolution of flow-through flaw: a, b, c, d – are the finite element simulation results ; e – is the photo of upper part of sample with a flow-through flaw: 1 – is the press-washer, 2 – is the porous fibrous pressing

The highest depth of flow-through flaw of 35 mm was reached at extrusion with λ = 16.8 (Fig. 3.10, a) and its volume was about 350 mm^3. The maximal volume of flow-through flawV_{sk} obtained at λ = 3.6 (Fig. 3.10, a) and its depth was minimal, 12-15 mm.
A comparison of theoretical and approximate experimental dependences of depth of flow-through flaw l_{sk} (Fig. 3.10) and height of loosening from the other end of sample h_{raz} (Fig. 3.11) from value of λ has shown that l_{sk} and h_{raz} are significantly growing while increasing of λ that diminishes useful length of sample l^{pr} :

$$l^{pr} = l_0^{pr} - l_{sk} - h_{raz}, \tag{3.2}$$

where l_0^{pr} - is the general length of rod.

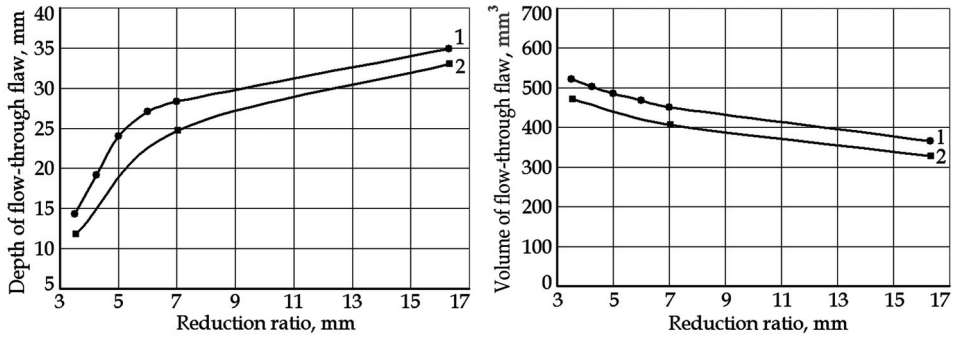

Fig. 3.10. The maximal depth and volume of flow-through flaw: a- is the dependence $l_{sk}(\lambda)$; b- is the dependence $V_{sk}(\lambda)$: 1- are theoretical dependences; 2- are experimental dependences

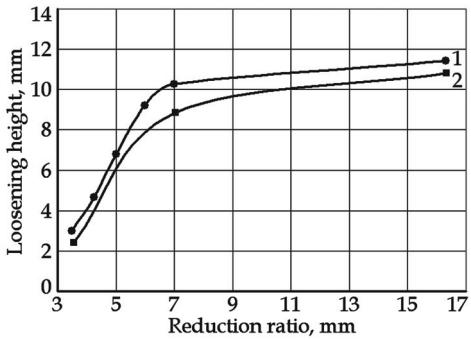

Fig. 3.11. The loosening height: 1 – is the theoretical dependence; 2 – is the experimental dependence

The shape of curves (Fig. 3.10, 3.11) indicates on possibility of their approximation by dependences that are taking into account an influence of non-uniformity of stress-strain state on the volume of flow-through flaw. The effective method of flow-through flaw removal is implementation of billet with compensator (Fig. 3.12). The followings empiric formulas for determination of compensator dimensions have obtained using processing of experimental data by a least-squares method and simulation results:

$$h_{sf} = 2\xi\lambda h_{pr}, \quad r_{sf} = (1.0\text{-}1.7\xi\lambda)D_{pr}, \tag{3.3}$$

where ξ - is the coefficient of non-uniformity of deformation (for copper fibres ξ = 1.02–1.17);
h_{sf} - is the height of compensator;
r_{sf} - is the radius of sphere of compensator;
D_{pr}, h_{pr} - are diameter and height of pressing.
Thus, the stress-strain state at direct extrusion of fibrous pressing is fully determined by reduction ratio. At the reduction ratio λ = 16.8 was produced a compact copper material due to shear stress value exceeding the critical shear stress at high hydrostatic pressure within 1050-1380 MPa that indicates to complete consolidation of fibres. The conditions of temperatures distribution by section of pressing are most hard at λ = 16.8 because of diminishing size of deformation zone and increasing the heat emission to the instrument.

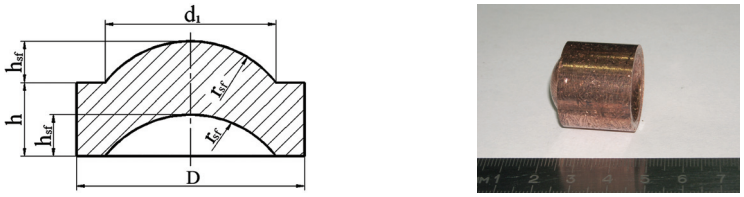

a) b)

Fig. 3.12. The draft of axial section of fibrous pressing with compensator (a) and photo (b)

The dependences for dimensions of defects (flow-through flaw and loosening) in the sample from deforming conditions have been determined. The analytical dependences for dimensions of initial pressing with compensator taking into account a volume of flow-through flaw were obtained and comparing with experimental dependences provided. The results of different methods are corresponding to each other with error less than 10%.

3.4 Modelling of extrusion of porous fibrous pressing with compensator

The investigation of stress-strain state at direct extrusion of porous fibrous pressing with spherical compensator, the reduction ratio λ = 16.8. The finite element model of extrusion of fibrous pressing with compensator is presented on Fig. 3.13. The height of compensator was accepted of 5 mm.

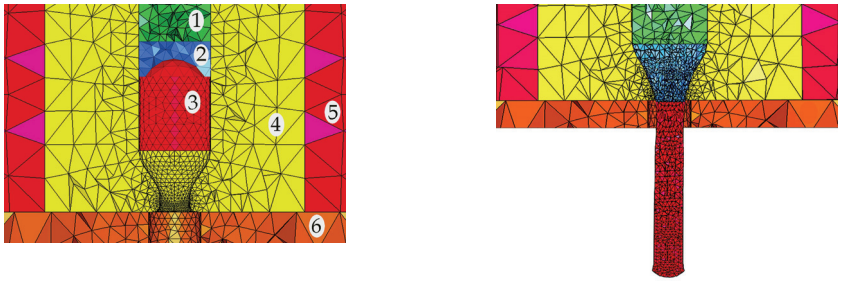

a) b)

Fig. 3.13. The finite element model of extrusion of fibrous pressing with compensator:
a- is the beginning of extrusion; b- is the end of extrusion: 1- is the upper puncheon; 2- is the press-washer; 3- is the initial pressing; 4- is the matrix; 5- is the bandage; 6- is the lower plate

The analysis of distributions of stress intensity and hydrostatic pressure (Fig. 3.14) has shown that type of curves remains analogical to dependences presented on Fig. 3.3. The presence of compensator on pressing provided increasing of stress intensity and hydrostatic pressure in sections 1-1 and 2-2. The hydrostatic pressure in section 3-3 became lower.

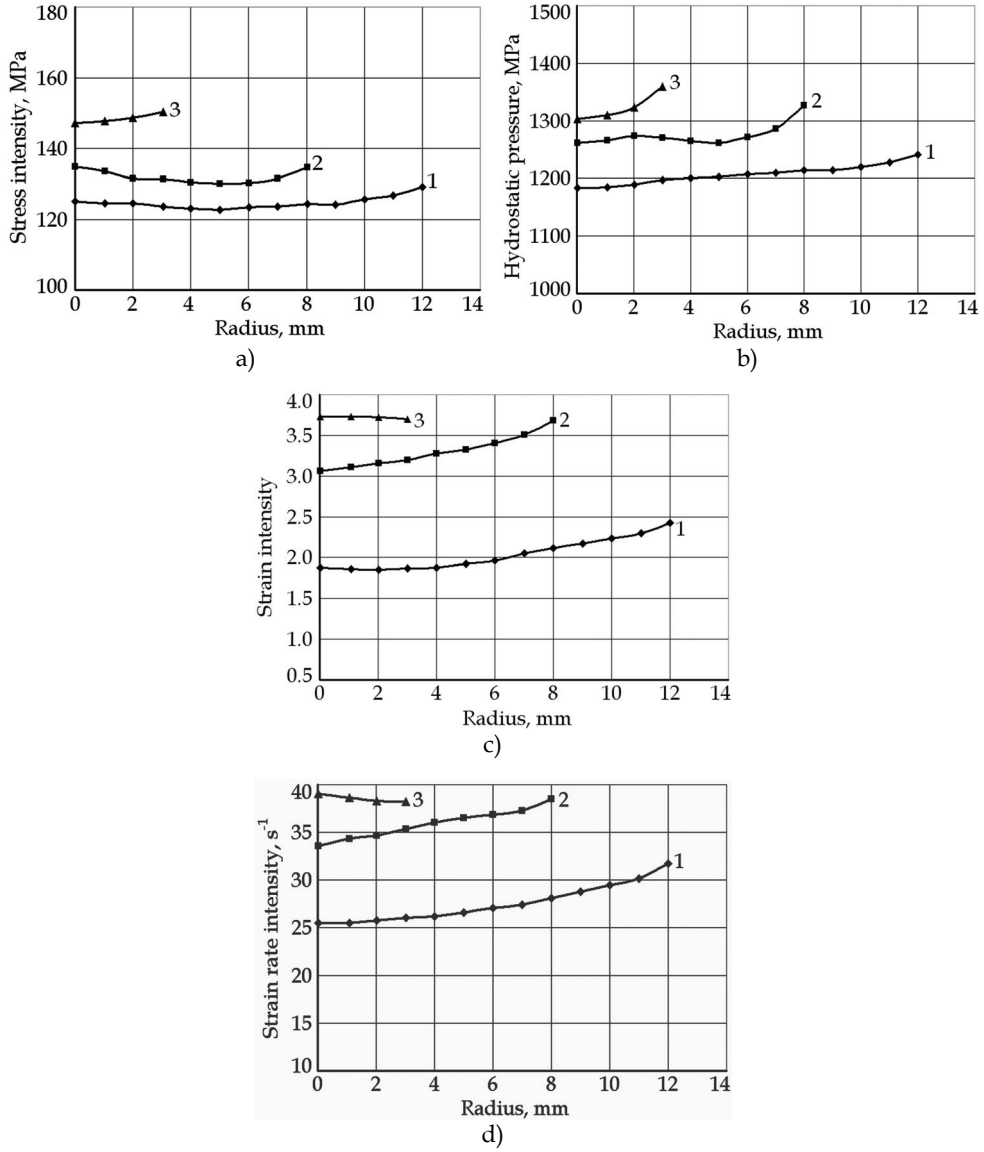

Fig. 3.14. The distribution of stress intensity (a), hydrostatic pressure (b), strain intensity (c), strain rate intensity (d) at extrusion with λ = 16.8: 1– is the section 1-1; 2 - is the section 2-2; 3 - is the section 3-3

There are no inflection points on curves corresponding to beginning formation of flow-through flaw (Shtern et al., 1982; Ryabicheva & Usatyuk, 2006). The distribution of hydrostatic pressure on the section of sample is more uniform. Obviously, the presence of compensator did not exert influence on shear stress intensity. The intensity of deformations is considerably growing in sections 1-1 and 2-2 in the places adjoining to compensator, especially on the axis of pressing (Fig. 3.14, c). The intensity of strain rate was considerably increased too (Fig. 3.14, d).
Thus, the presence of compensator, located on the axis of pressing, resulted to increase of stress intensity and deformations intensity and ensured the removal of flow-through flaw. It has established that deformation takes place more intensively in the area of compensator due to the primary contact of pressing has carried out with press-washer and then with other surface.

3.5 Investigation of plasticity resource

Solving the technological problems of production of fibrous materials coupled with investigation of plasticity resource that is changing under the influence of temperature and strain rate conditions of deformation and is one of criteria for estimation of quality of wares during finite element modelling of direct extrusion of porous fibrous pressings.
The criteria for estimating of plasticity resource were offered on the basis of stress tensor invariants according to (Ogorodnikov et al., 2005). The quantitative relation between ultimate deformation and parameters of stress-strain state is a diagram of plasticity. In such case stiffness of the stress-strain state described by Lode coefficient η_l and exerts influence on plasticity:

$$\eta_l = \frac{\sigma_1 + \sigma_2 + \sigma_3}{\sigma_i}. \tag{3.4}$$

The type of stress-strain state is determined by the Nadai-Lode stress parameter μ_σ that allows estimating an influence of middle main stress on plasticity (Ogorodnikov et al., 2005):

$$\mu_\sigma = \frac{2\sigma_2 - \sigma_1 - \sigma_3}{\sigma_1 - \sigma_3}. \tag{3.5}$$

In such case the measure of plasticity is ultimate deformation that may be determined for any deformed material from a diagram of plasticity built using results of three tests – tension, compression and torsion (Ogorodnikov et al., 2005).
These above mentioned parameters are taking into account of hydrostatic pressure exerting the influence on plasticity, and stress intensity that are determining the plastic flow of material and, also, characterizing the stiffness of stress-strain state. However they are not taking into account the influence of the third invariant of stress tensor.
In the papers (Ogorodnikov et al., 2005; Ogorodnikov et al., 2007) have proposed to construct the diagram of plasticity as a surface of ultimate deformations in space of dimensionless parameters η_l and μ_σ - $e_p(\eta_l, \mu_\sigma)$ for investigation of plasticity resource at the volumetric stress-strain state. During construction of such diagrams the type of loading trajectories and ultimate deformations are simply defined by a deformation scheme and are not depend on properties of material. Therefore, a general view of plasticity resource criterion is presented by following expression (Ogorodnikov et al., 2005):

$$\Psi = \int_0^{e_i} n \frac{e_i^{n-1}}{e_p(\eta_l, \mu_\sigma)^n} de_i \le 1, \tag{3.6}$$

where e_P – is the ultimate deformation at fracture,

e_i – is the intensity of deformations,

$e_P(\eta_l, \mu_\sigma)$ – is the surface of ultimate deformations,

$n = 1 + 0.2 \operatorname{arctg}\left(\frac{d\eta_l}{de_i}\right)$ – is the index that takes into account a character of plasticity changing depends on stiffness of stress-strain state.

In the paper (Ogorodnikov et al., 2005) the following dependence was proposed for approximation of surfaces of ultimate deformations:

$$e_P(\eta_l, \mu_\sigma) = \frac{e_P(0,0)\exp(-b\eta_l)}{1 + \lambda_1 \mu_\sigma + \lambda_2 \mu_\sigma^2}, \tag{3.7}$$

where $\lambda_1 = \ln\left(\frac{e_p(-1,0)}{e_p(0,0)}\right)$, $\lambda_2 = \ln\left(\frac{e_p(0,1)}{e_p(0,0)}\right)$, $b = \lambda_1 - \lambda_2$ - are approximation coefficients;

$e_P(0,0)$ - is the ultimate deformation at torsion test;

$e_P(-1,0)$ - is the ultimate deformation at compression test;

$e_P(0,1)$ - is the ultimate deformation at tension test.

The following values of ultimate deformations were determined by the results of mechanical tests on torsion, compression and tension of material obtained by hot extrusion of fibrous pressing (Fig. 3.15): $e_P(0,0) = 0.62$; $e_P(-1,0) = 0.83$; $e_P(0,1) = 0.75$. The strain rate was 0.1 min^{-1} according to GOST 1497-84.

Construction of surface of ultimate deformations using expression (3.7) makes necessary implementation of strain rate coefficient E_λ that is taking into account the difference in strain rates at mechanical tests and hot extrusion:

$$E_\lambda = \frac{\dot{\varepsilon}_{test}}{\dot{\varepsilon}_{def}}, \tag{3.8}$$

where $\dot{\varepsilon}_{test}$ - is the strain rate at the mechanical tests;

$\dot{\varepsilon}_{def}$ - is the average strain rate in the process of direct extrusion.

After substitution of formula (3.8) to the expression (3.7) obtained:

$$\lambda_1 = E_\lambda \ln\left(\frac{e_p(-1,0)}{e_p(0,0)}\right), \quad \lambda_2 = E_\lambda \ln\left(\frac{e_p(0,1)}{e_p(0,0)}\right). \tag{3.9}$$

Therefore, $\lambda_1 = 1.93 \cdot 10^{-5}$, $\lambda_2 = 1.27 \cdot 10^{-5}$, $b = 0.1$.

Substituting values from (3.9) to (3.7) having the following expression:

$$e_P(\eta_l, \mu_\sigma) = \frac{0.62\exp(-0.1\eta)}{1 + 1.93 \cdot 10^{-5}\mu_\sigma + 1.27 \cdot 10^{-5}\mu_\sigma^2}. \tag{3.10}$$

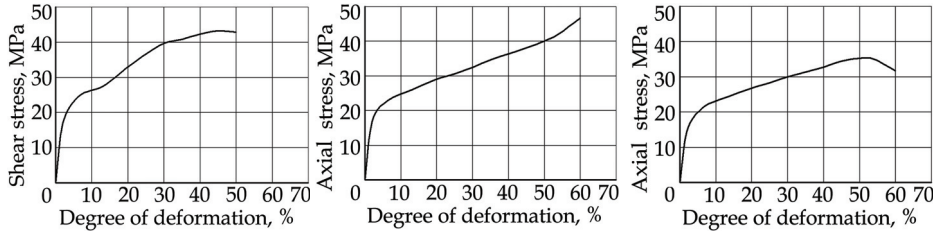

Fig. 3.15. Flow curves: a – at torsion; b – at compression; c – at tension

The dependence of Lode coefficient from intensity of deformations may be obtained by numerical differentiation of (3.4) by e_i for any point of fibrous pressing, if $\eta_l(e_i)$ at interval $[0, e_P]$ continuously differentiable and integrable. This dependence is velocity of changing the stiffness of stress-strain state at hot extrusion and may be decomposed into the trigonometric series that looks like:

$$\frac{d\eta_l}{de_i} = \frac{a_0}{2} + \sum_{k=1}^{\infty} a_k \cos(e_i) + b_k \sin(e_i)\,, \tag{3.11}$$

where $a_0, a_k = \frac{1}{e_i}\int_0^{e_i} \eta_l(e_i)\cos(k\pi e_i)de_i$, $b_k = \frac{1}{e_i}\int_0^{e_i} \eta_l(e_i)\sin(k\pi e_i)de_i$ – are coefficients.

In the initial moment at $e_i = 0$, $\eta_l(e_i) = 0$ and $\frac{d\eta_l}{de_i} = 0$, therefore $a_0 = 0$ and series (3.11) for the copper porous fibrous pressing may be written in the following way:

$$\frac{d\eta_l}{de_i} = \sum_{k=1}^{\infty} a_k \cos(e_i) + b_k \sin(e_i)\,. \tag{3.12}$$

After substitution of expressions (3.10), (3.11) and (3.12) to (3.6), it looks like:

$$\Psi = \int_0^{e_i} n \frac{e_i^{n-1}}{\left(\frac{0.62\exp(-0.1\eta_l)}{1 + 1.93\cdot 10^{-5}\mu_\sigma + 1.27\cdot 10^{-5}\mu_\sigma^2}\right)^n} de_i \le 1\,, \tag{3.13}$$

where $n = 1 + 0.2\,\mathrm{arctg}\left(\sum_{k=1}^{\infty} a_k \cos(e_i) + b_k \sin(e_i)\right)$.

Analytical integration of expression (3.13) for obtaining the expression that characterizing a plasticity resource of material at any point of fibrous pressing during passing through the deformation zone is impossible. Numeral integration of expression (3.13) has performed by computer using Mathcad 12. Integration results are presented on Fig. 3.16, curve 1.

Decomposition of function (3.13) in a power-law series have done for saving of computational resources while investigation of plasticity resource in points of fibrous pressing:

$$\Psi = ae_i + \frac{ae_i^2}{2!} - \frac{ae_i^3}{3!} + \frac{ae_i^4}{4!} - \frac{ae_i^5}{5!} + \frac{ae_i^6}{6!} - \frac{ae_i^7}{7!} + \ldots\,, \tag{3.14}$$

where a – is the coefficient of power-law series.
During extrusion of porous fibrous pressing a = 0.02, then, substituting a in (3.14), calculating factorials and limited to the first seven terms of series having the following expression:

$$\Psi = 0.02e_i + \frac{0.02e_i^2}{2} + \frac{0.02e_i^3}{6} + \frac{0.02e_i^4}{24} + \frac{0.02e_i^5}{120} + \frac{0.02e_i^6}{720} + \frac{0.02e_i^7}{5040}. \quad (3.15)$$

The results of determination of plasticity resource by formula (3.15) are presented at Fig. 3.16, curve 2. The investigation of plasticity resource performed for points located on the axis of pressing while passing through the deformation zone at the reduction ratio $\lambda = 16.8$ shown that for the given deformation conditions the value of $\lambda = 16.8$ is ultimate because of providing the complete consolidation of fibres and exhausting of more then a half of plasticity resource $\Psi = 0.55–0.62 < 1$. Consequently, improving of extrusion productivity by increasing of deforming velocity over 0.5 m/s is not possible. A surface that characterizing intensity of deformations of points of fibrous pressing at hot extrusion $e_i(\eta_l, \mu_\sigma)$ does not intersect the surface of ultimate deformations $e_p(\eta_l, \mu_\sigma)$ (Fig. 3.17) described by expression (3.13).

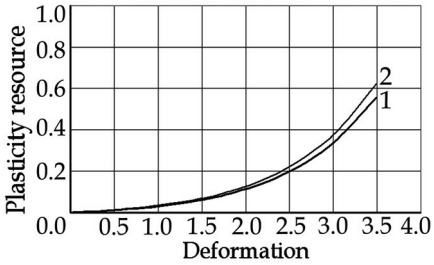

Fig. 3.16. Determination of plasticity resource of points on the axis of fibrous pressing:
1 – obtained by numerical integration of expression (3.13); 2 – according to formula (3.15)

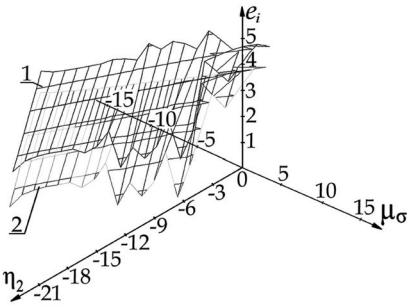

Fig. 3.17. Surfaces of deformations: 1 - is the surface of ultimate deformations; 2 - is the surface of deformations intensity

Comparing values of plasticity resource obtained by numerical integration of expression (3.13) and by using formula (3.15) has shown that they corresponding to each other with relative error 7-11%.

3.6 Modelling of physico-mechanical properties of single-component fibrous material

Finite element modelling of compression test for estimating of physical and mechanical properties of single-component copper fibrous material has been performed.
The initial data are physical and mechanical properties of compact material and value of initial porosity (Table 3.1).

Component	Density, kg/m^3	Initial porosity, %	Young modulus, MPa	Poisson's ratio	Yield stress, MPa	Ultimate stress, MPa
Copper	8940	21	$1.20 \cdot 10^5$	0.33	120	220

Table 3.1. Initial data

The production technique	Ultimate stress, MPa	Yield stress, MPa	Relative elongation, δ,%	Contraction ratio, ψ,%	Hardness, HB
Hot stamping of fibrous pressings, cold deforming, annealing	218.7	45.7	37.5	40.5	55-60

Table 3.2. Mechanical properties of copper fibrous pressing

Material	Kind of data	Porosity, %	Density, kg/m^3	Young modulus, MPa	Poisson's ratio	Relative elongation, δ, %	Yield stress, MPa	Ultimate stress, MPa
Copper	S	5	8490	$1.1 \cdot 10^5$	0.45	38	240	360
	E	3	8670	$1.2 \cdot 10^5$	0.41	40	255	380

S – are simulation results; E – are experimental results.

Table 3.3. Calculated and experimental properties of copper fibrous material after extrusion

3.7 Modelling of physico-mechanical properties of multi-component powder material

Production of antifriction materials with given properties makes necessary investigation the influence of temperature, degree of deformation and strain rate at densification of heterogeneous powder material. The basis of materials observed in this investigation is copper powder obtained from wastes of copper current conductors and ligature is nickel powder produced by recycling of wastes from cadmium-nickel batteries.
The initial data for determination of properties of multi-component copper-based porous powder material are presented in Table 3.4. The finite element model of the multi-component material, the analytical model of compression test and distribution of density are presented on Fig. 3.18, a.
The technology for production of samples consists of the following operations: moulding of powder mixture, sintering at 950 ^{0}C into the synthesis-gas medium for 3.5 hours (the gas composition is 72% H_2, 21% CO, 5.5% CO_2, 1.5% H_2O), repeated moulding up to porosity 10, 20 and 30 %, homogenizing annealing into the synthesis-gas medium at 960 ^{0}C for 1 hour, hardening in water (Ryabicheva et al., 2008).

N	Component	Volume fraction, %	Density, kg/m^3	Young's modulus, MPa	Poisson's ratio	Yield stress, MPa	Ultimate stress, MPa
1	Copper	70-90	8940	$1.20 \cdot 10^5$	0.33	120	220
2	Nickel	10–30	8897	$2.03 \cdot 10^5$	0.31	210	450
3	Cobalt	5	8900	$2.09 \cdot 10^5$	0.31	200	350
4	Iron	2	7850	$2.10 \cdot 10^5$	0.28	200	280
5	Manganese	1	7470	$1.98 \cdot 10^5$	0.22	210	430
6	Titanium	3	4505	$1.10 \cdot 10^5$	0.34	160	530
7	Graphite	1	1800	$0.85 \cdot 10^5$	0.43	100	120
8	Porosity	10–30	0	0.00	1.00	0	0

Table 3.4. The components of multi-component material and their initial properties

The densification process of multi-component powder materials at elevated temperatures is going with shifting of elementary volumes of porous body mainly on phases interface boundaries or «soft» phase. The elements of hard phase are acting like dense bodies. Complex composition of ligature makes an influence on the deforming process. A graphite, for example, does not interacts with copper, remains at free state and may be a hard lubricant on the one part and stress concentrator on the other part diminishing strength and plasticity of antifriction material (Tumilovich et al., 1992; Ryabicheva et al., 2008).

Investigation the influence of degree of deformation and strain rate on densification of heterogeneous powder material at the elevated temperature interval has shown that density is growing the more intensively the higher is strain rate, while increasing the degree of deformation. The most intensive deformation of metal is taking place in deformation zone located in the central part of sample. When stress intensity in hard phase reached the yield stress, the deformation embracing the whole volume of sample. The hardness is higher in zones of higher deformation due to hardening (Ryabicheva et al., 2008).

Metal particles in peripheral ring zone are moving at the radial direction. The shear tensile stresses are arising in it. The hardness is growing while shifting away from periphery of sample that densificating considerably less and is a place of formation of first cracks while reaching the ultimate degree of deformation. The central part of sample is densificating most intensively at the expense of compression stresses and peripheral part less intensively due to metal flow in the radial direction. The condition of reaching the ultimate density is ultimate degree of deformation (Krashchenko & Statsenko, 1981; Ryabicheva et al., 2008).

A transverse flow of metal in the volume of central part have begun after reaching of ultimate degree of deformation and peripheral part is densificating at the expense of central part that becoming smaller. It is impossible to reach full densification in such conditions because of fracturing a surface of sample (Ryabicheva et al., 2008).

It is well-known that higher density of powder material may be reached at higher strain rates and equal degrees of deformation. It has been established experimentally that density of samples is growing up to ultimate while increasing the degree of deformation (Fig. 3.10), and density obtained at strain rate 10 s^{-1} is higher then density of samples upset at strain rate 0.1 s^{-1} at the same degrees of deformation (Ryabicheva et al., 2008).

The initial data for determination of properties of multi-component copper-based porous powder material are presented in Table 3.4. The finite element model of the multi-component material, the analytical model of compression test and distribution of density are presented on Fig. 3.18, a.

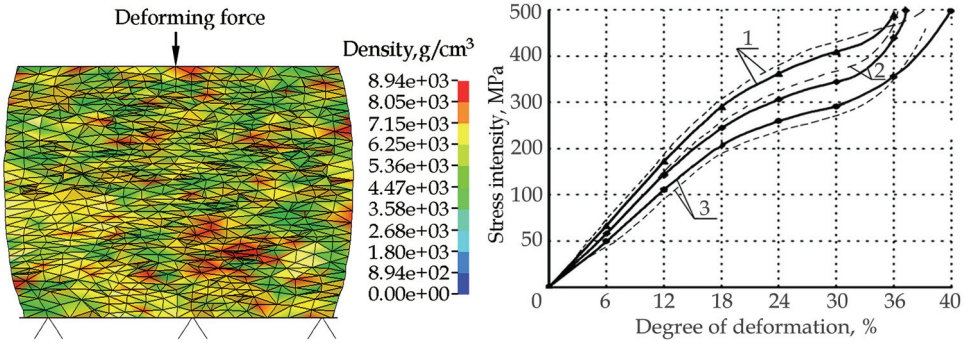

Fig. 3.18. The finite element model of the multi-component material, analytical model, density distribution (a), stress-strain dependences (b): 1 – is material 1; 2 – is material 2; 3 – is material 3: ▬▬ – are simulation results; - - - - - – are experimental results

Material	Volume fraction, %		Type of data	Porosity, %	Density, kg/m³	Young's modulus, MPa	Poisson's ratio	Ultimate strain, %	Yield stress, MPa	Ultimate stress, MPa
	Copper	Nickel								
Material 1	90	10	S	10	8046	$1.53 \cdot 10^5$	0.42	34	320	430
			E	8	8110	$1.65 \cdot 10^5$	0.40	36	340	460
Material 2	80	20	S	20	7152	$8.75 \cdot 10^4$	0.38	30	280	370
			E	17	7350	$9.15 \cdot 10^4$	0.35	33	300	390
Material 3	70	30	S	30	6560	$5.86 \cdot 10^4$	0.35	30	250	300
			E	32	6245	$5.56 \cdot 10^4$	0.31	28	230	270

S – are simulation results; E – are experimental results.

Table 3.5. Properties of multi-component copper-based powder materials

The laboratory experiments of compression tests are planned and carried out on the basis of numerical simulation results. The stress-strain dependences are drawn using the simulation and experimental results that are in concordance (Fig. 3.18, b). The relative inaccuracy of mathematical and experimental investigation of properties does not exceed 10%.

It has established that highest level of mechanical properties is shown by material 1 due to its lowest porosity. The material 3 has lowest mechanical properties (Table 3.5) because of highest porosity and, moreover, interparticle cracks may appear on copper-nickel boundaries due to significant difference of their strength properties. Thus, decreasing of porosity on 20% promotes to increasing of strength properties on 40%.

4. Conclusion

It has established that stress-strain state and temperature fields at extrusion of fibrous pressing are fully determined by the reduction ratio. A compact copper material was produced at the reduction ratio λ=16.8 and high hydrostatic pressure within 1050-1380 MPa. The shear stress value exceeded the critical shear stress that indicates on complete consolidation of fibres.

Conditions of formation of defects during extrusion of fibrous pressing have determined. The analytical dependences for determining dimensions of initial pressing with a compensator with taking into account dimensions of defects have proposed.

The presence of compensator located on the axis of pressing led to increasing of stress intensity and intensity of deformations and ensured defects' removal. It has established that near compensator deformation is taking place more intensively due to the primary contact of pressing has carried out with press-washer and then with other surface.

Investigation of plasticity resource of points located on the axis of pressing while passing through the deformation zone at the reduction ratio $\lambda = 16.8$ shown that for the given deformation conditions the value of $\lambda = 16.8$ is ultimate because of providing the complete consolidation of fibres and exhausting of more then a half of plasticity resource $\Psi = 0.55\text{-}0.62 < 1$. Consequently, improving of extrusion productivity by increasing of deforming velocity over 0.5 m/s is not possible.

A surface that characterizing intensity of deformations of points of fibrous pressing at hot extrusion $e_i(\eta_l, \mu_o)$ does not intersect the surface of ultimate deformations $e_p(\eta_l, \mu_o)$.

The technique for finite element modelling of physical and mechanical properties of single-component fibrous material with taking into account properties of fibres' material in compact state and deforming conditions that allows defining conditions of complete consolidation of fibres at the deforming process using the stress-strain state analysis results of fibrous pressing at the deforming process has been developed.

The technique for modelling of physical and mechanical properties of multi-component powder materials using a finite element method on the basis of physical and mechanical properties of initial components while accounting deforming conditions has been developed. The distribution of density of multi-component powder material in the volume of sample obtained.

The influence of nickel content and porosity value on mechanical properties of material has been established. Increasing of nickel content leads to enhancing of strength properties. The content of other components and their influence on properties was accounted by interaction of finite elements. Growth of porosity leads to decreasing of mechanical properties. The results of modelling physical and mechanical properties of multi-component powder materials are well concordant with the results of the laboratory experiments.

5. References

Hallquist, J. O. (2006). *LS-DYNA Theory Manual,* Livermore Software Technology Corporation, ISBN 0-9778540-0-0, Livermore.

Kachanov, L. M. (1969). *The Basics of Plasticity Theory*, Nauka, Moscow.

Krashchenko, V. P. & Statsenko, V. E. (1981). Effect of temperature and strain rate on basic processes controlling the strength of copper, *Strength of Materials*, Vol. 13, No. 4, pp. 487-492, ISSN 0039-2316.

Ogorodnikov, V. A.; Kiselev, V. B. & Sivak, I. O. (2005). *Energy. Deformation. Fracture.,* Universum-Vinnitsa, ISBN 966-641-117-2, Vinnitsa.

Ogorodnikov, V. A.; Muzichuk, V. I. & Nahajchuk, O. V. (2007). *The mechanics of cold shaping processes with equitype schemes of deformation mechanism,* Universum-Vinnitsa, ISBN 978-966-641-217-4, Vinnitsa.

Petrosjan, G. L. (1988). Plastic deformation of powder materials, Metallurgy, ISBN 5-229-00160-7, Moscow.

Ryabicheva, L. A. & Usatyuk, D. A. (2006). Using the finite element method for solving of coupled thermal-structural problem, *Herald of the DSEA*, No. 3, pp. 141-147, ISSN: 1993-8322.

Ryabicheva, L. & Usatyuk, D. (2007). Numerical Simulation and Forecasting of Mechanical Properties for Multi-Component Nonferrous Dispersion-Hardened Powder Materials, *Materials Science Forum*, Vols. 534-536, pp. 397-400, ISSN: 1662-9752.

Ryabicheva, L. A. & Nikitin, Yu. N. (2008). Production and properties of copper-based powder antifriction material, *Powder Metallurgy and Metal Ceramics,* Vol. 47, No. 5-6, pp. 299-303, ISSN: 1573-9066.

Ryabicheva, L. A.; Tsyrkin, A. T. & Sklyar, A. P. (2008). Production and properties of copper-based compacts, *Powder Metallurgy and Metal Ceramics,* Vol. 47, No. 7-8, pp. 414-419, ISSN: 1573-9066.

Segal, V. M.; Reznikov, V. I. & Malyshev, V. F. (1981). Variational functional for a porous plastic body, *Powder Metallurgy and Metal Ceramics,* Vol. 20, No. 9, pp. 604-607, ISSN: 1573-9066.

Skorokhod, V. V. (1973). *The rheological basics of sintering theory*, Naukova Dumka, ISBN 5-7695-2294-1, Kiev.

Shtern, M. B.; Serdyuk G. G. & Maximenko L.A. (1982). *Phenomenological Theories of Pressing of Powders,* Naukova Dumka, Kiev.

Tumilovich, M. V.; Kostornov, A. G.; Leonov, A. N.; Sheleg, V. K. & Kaptsevich, V. M. (1992). Porous copper-base fiber-powder materials, *Powder Metallurgy and Metal Ceramics,* Vol. 31, No. 3, pp. 239-242, ISSN: 1573-9066.

Wagoner, R. H. & Chenot, J. L. (2001). *Metal Forming Analysis,* Cambridge University Press, ISBN 0-521-64267-1, Cambridge.

Zienkiewicz, O. C. & Taylor, R. L. (2000). *The Finite Element Method,* Butterworth-Heinemann, ISBN 0-7506-5049-4, Barcelona.